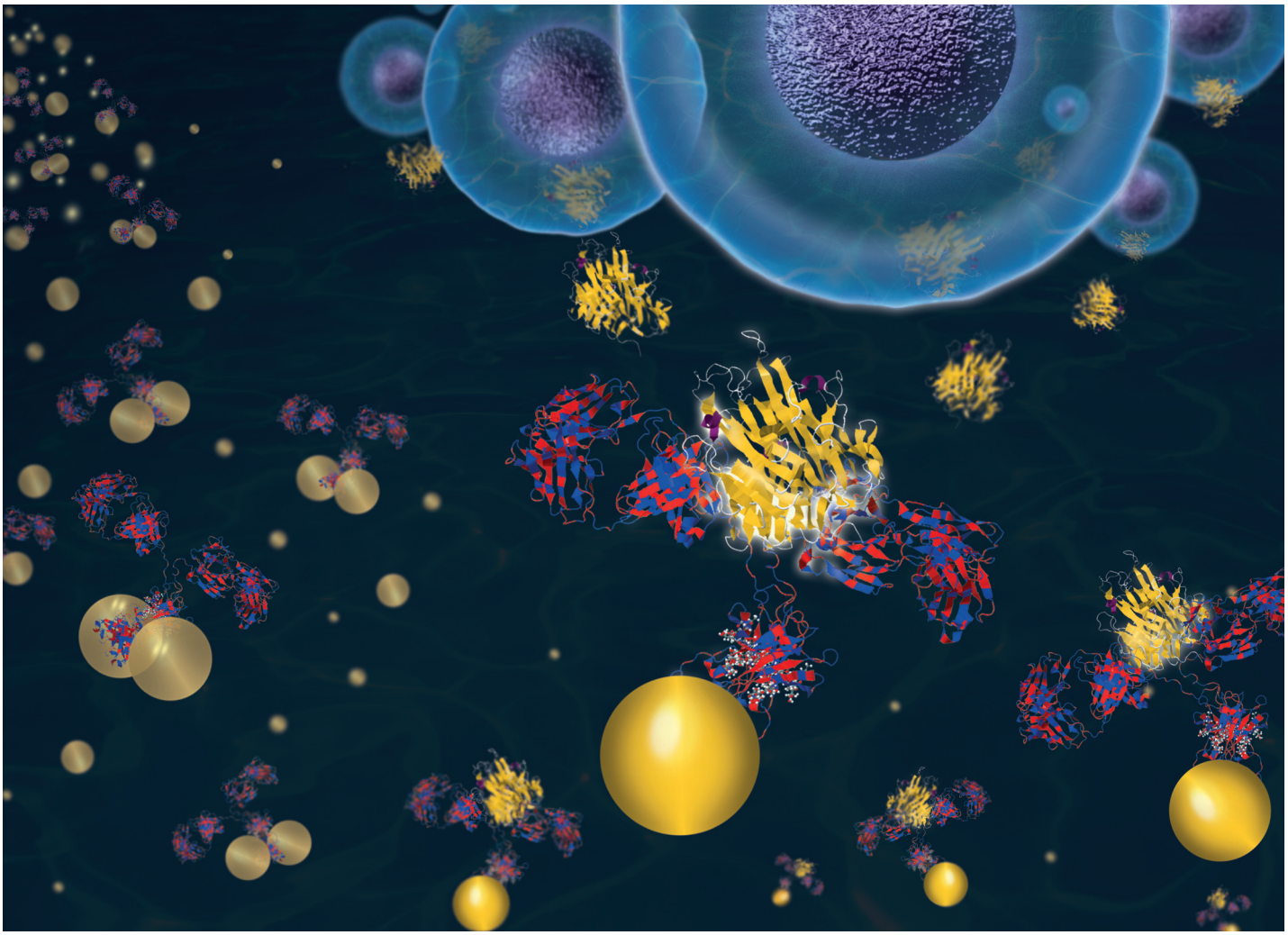

Showcasing research from Departments of Physical Chemistry (INFIQC) and of Clinical Biochemistry (CIBICI), School of Chemistry, National University of Córdoba and National Scientific and Technical Research Council (CONICET), Córdoba, Argentina. Illustration: J. Di Pietro, Institutional Relations, (CCT-CONICET-Córdoba).

Design of a novel plasmonic nanoconjugated analytical tool for ultrasensitive antigen quantification

We present a novel ultrasensitive optical bionanosensor with a widespread capability of antigen detection. The biosensor is based on the controlled agglomeration of functionalized Ag nanospheres generated in the presence of a biotinylated immunoglobulin acting as a linker between these nanoparticles and for the inhibition of agglomeration in the presence of the antigen. The change in the intensity of the UV-Vis spectra is very sensitive to the antigen concentration with a sensibility 100 times greater than the standard ELISA.

As featured in:

See Juan C. Fraire, Eduardo A. Coronado *et al.*, *Nanoscale*, 2016, **8**, 17169.

ROYAL SOCIETY OF CHEMISTRY

www.rsc.org/nanoscale

Registered charity number: 207890

Nanoscale

PAPER

Cite this: *Nanoscale*, 2016, **8**, 17169

Design of a novel plasmonic nanoconjugated analytical tool for ultrasensitive antigen quantification†

Juan C. Fraire,*[a] Ruben D. Motrich[b] and Eduardo A. Coronado*[a]

Received 17th June 2016,
Accepted 15th July 2016

DOI: 10.1039/c6nr04897h

www.rsc.org/nanoscale

To date, while various diagnostic approaches for antigen detection have been proposed, most are too expensive, lengthy and limited in sensitivity for clinical use. Nanoparticle systems with unique material properties, however, circumvent these problems and offer improved accuracy and sensitivity over current methods like the enzyme-linked immunosorbent assay (ELISA). Herein, we present a novel functionalization strategy of plasmonic nanoparticle probes capable of specific quantification of antigens directly in clinical samples. A nanoconjugation strategy that allows one to perform an intensity depletion immunolinked assay (IDILA), involving specific antibodies that target the antigen of interest was designed to obtain a calibration curve and achieve the quantification of the antigen in clinical samples in the same experiment using a microplate reader (*i.e.*, an UV-vis spectrophotometer). Finally, the IDILA methodology allowed specific detection of various clinically relevant antigens, with significantly improved sensitivity over the ELISA. Furthermore, the assay was shown to be robust, reliable, cheap and rapid, diagnosing antigens in clinical serum samples within 2 hours.

Introduction

Rapid and sensitive detection of antigens is crucial for early diagnosis of human diseases to improve patient care.[1,2] Early diagnosis and suitable therapy are therefore of decisive importance for the prognosis of any disease. The three pillars for diagnosis are the medical history, clinical findings (including imaging techniques) and serological laboratory tests.[3] To date, a variety of diagnostic approaches have been proposed for serological tests, each varying in sensitivity, specificity, cost, and efficacy.[2–4] In particular, strategies based on enzyme-linked immunosorbent assay (ELISA) are widely used as diagnostic tools in medicine for the detection and quantification of specific antigens or antibodies in a given sample. ELISA uses the basic immunology concept of an antigen binding to its specific antibody, which allows detection of very small quantities of antigens in a fluid sample. The antigen in a fluid phase is immobilized, usually in 96-well plates, to a specific antibody, which is itself subsequently detected by a secondary, enzyme-coupled antibody that yields a visible color change or fluorescence, indicating the presence of the antigen.[5–7] However, the ELISA methodology still has limitations due to nonspecific binding to the plate or to the enzyme-mediated color change reaction, that could lead to false positive results.[6] Moreover, it uses high amounts of reagents in the plate-immobilization-process, and requires several washing steps that are time consuming.[7] There is thus a need for generic, accurate and point-of-care platforms being capable of rapid and specific quantification of antigens directly in clinical samples.

Nanomaterials have some unique physical and chemical properties that are fundamentally different from those of the corresponding bulk material due to their small size.[8] They usually have a large surface–volume ratio and large amounts of different molecules can be easily labeled onto their surface. In particular, noble metal nanoparticles (NPs) have long been recognized for their unique optical properties as their plasmon resonance frequencies can be tuned just by changing geometrical parameters, such as nanoparticle size,[9] shape,[9] and particle–particle spacing.[10–13] In addition, their surface properties are suitable for developing several functionalization strategies involving biomolecules that could be specific linkers and also bio-recognition agents able to preferentially interact

[a]*INFIQC, Centro Laser de Ciencias Moleculares, Departamento de Fisicoquímica, Córdoba, 5000, Argentina. E-mail: jfraire@fcq.unc.edu.ar, coronado@fcq.unc.edu.ar*
[b]*CIBICI, Departamento de Bioquímica Clínica, Facultad de Ciencias Químicas, Universidad Nacional de Córdoba, Córdoba, 5000, Argentina*

†Electronic supplementary information (ESI) available: Theoretical simulations of the far-field optical response of Ag NS dimers; theoretical simulations of the far-field optical response of Au NS dimers; kinetics measurements of the dimer formation using a biotinylated goat anti-rabbit IgG antibody (Biot-IgG); kinetics measurements of the dimer formation using a biotinylated anti-IL-10 IgG antibody (Biot-IgG); structural parameters of the antigens used in this study; spectral stability of the Ag NP colloidal dispersion; comparison of methods for antigen quantification. See DOI: 10.1039/c6nr04897h

with target molecules.[14,15] NP-based assays have the potential to be used to detect events and processes in biological systems with unprecedented levels of sensitivity and localization (detection and quantification of cell membrane receptors,[15–17] studies of cellular processes,[18] cellular imaging,[19,20] *etc.*) improving the sensitivity and specificity of medical testing and providing new tools for clinical diagnosis.[21–25]

We report here a new sensing platform for rapid detection and quantification of antigens in real samples using protein-functionalized plasmonic NPs and antibodies. Because the detection is based on the optical properties of the colloidal dispersion of linked plasmonic NPs, the proposed method allows sensing without any signal perturbation due to the immobilization of reagents or uncontrolled enzymatic reactions, the assay steps are greatly simplified and detection is much faster, in comparison with the standard ELISA. In this work, the principles of a new method that will be denoted as NP-based intensity depletion immuno-linked assay (IDILA) are outlined. The robustness of the method is shown by testing several antigens, and finally the application of the method for the sensing performance with serum of rheumatoid arthritis (RA) patients is demonstrated (RA is one of the most common chronic inflammatory autoimmune diseases with a prevalence of about 0.5%–1% and an incidence of about 30 per 100 000 inhabitants).[3] For a signal readout, we use a common UV-Vis spectrometer and we evaluate the applicability of the method using standard equipment commonly used to perform ELISA (microplate reader), showing that IDILA requires smaller volumes of sample for processing and is capable of supporting rapid operation. In particular, we demonstrate that this methodology could be used to detect several cytokines, which play an important role in the activation, proliferation and differentiation of B and T cells, macrophages, dendritic cells, granulocytes and various other cells that participate in the immune response and that have been implicated in the pathogenesis of RA.[26]

Materials and methods

Materials

The following materials were used as obtained: $AgNO_3$ (J. T. Baker, Phillipsburg, NJ, USA); sodium citrate (Mallinckrodt, St Louis, MO, USA); EZ-Link Biotin-HPDP (Pierce Thermo Scientific, Waltham, MA, USA); streptavidin (Invitrogen, Carlsbad, CA, USA); rabbit polyclonal anti-c-Myc IgG (Santa Cruz Biotechnology, Inc., Santa Cruz, CA, USA); biotin-conjugated goat anti-rabbit IgG antibody (Molecular Probes, Inc., Eugene, OR, USA); biotin-conjugated rat anti-mouse IFNγ antibody (BD Biosciences, San Diego, CA, USA); biotin-conjugated rat anti-mouse IL-10 antibody (BD Biosciences, San Diego, CA, USA); biotin-conjugated rat anti-human TNFα antibody (BioLegend, San Diego, CA, USA).

Ag nanospheres synthesis

The synthesis of silver nanoparticles was performed using the Turkevich method, which is based on the reduction properties of boiling citrate solutions. Ag NSs were obtained by reducing a 50 mL of 0.2 mM silver nitrate solution ($AgNO_3$) with the addition of 1 mL of a 0.01 M citrate solution (corresponding to a 1 : 1 Ag/citrate molar ratio) under heat and rapid stirring for 30 min. The morphological characterization of Ag NSs was performed combining UV-vis spectroscopy, TEM, and electrodynamics modeling using Mie theory. The overall results after combining all of these different techniques and modeling indicate that the average diameter was 60 nm with a concentration of 4.57×10^9 NSs per cm^3 (7.59×10^{-12} M) for Ag NSs. The concentration of Ag nanoparticles was estimated to be around 7 pM, using the experimental extinction intensities at the maximum wavelength, and Mie theory calculations of the extinction cross section for spherical particles with the corresponding diameter (determined by TEM). It is important to note that Ag NPs can be easily purchased and it is not necessary to synthesize them.

Particle functionalization

EZ-Link Biotin-HPDP (*N*-[6-(biotinamido)hexyl]-3′-(2′-pyridyldithio)propionamide) was used for surface modification of 60 nm Ag NSs. The procedure for the functionalization involves the incubation of the NS solution simultaneously with EZ-Link Biotin-HPDP and with streptavidin (STV) (molar ratio NSs/biotin/STV 1 : 1 : 1) for 1 h at room temperature.

Kinetics measurements

For the determination of the agglomeration rate constant (k_{Aglo}) for the dimer formation, 0.5 mL of the functionalized Ag NPs were added to 5% w/v BSA supplemented PBS (final volume of 1.5 mL). For experiments of the Biot-IgG concentration effect on k_{Aglo}, different amounts of Biot-IgG were added directly to the mixture of Ag NPs and the buffer. For experiments of the antigen concentration effect on k_{Aglo}, a specific amount of Biot-IgG (0.3 ng mL^{-1}) and different amounts of antigen were added directly to the mixture of Ag NPs and the buffer. The Biot-IgG concentration was chosen in order to be in the regime where dimer formation is favored. The spectral evolution was monitored with an UV-Vis spectrophotometer in the range of 300 nm to 1100 nm every 2 min for 20 min. The integral in the range of 340 nm to 800 nm was calculated for each spectrum, and then was plotted as a function of the Biot-IgG or antigen concentration, in order to obtain the k_{Aglo} values, respectively. In every case the linear fitting gave a R^2 value above 0.99.

Static measurements

Sample preparation for static measurements is exactly the same as for kinetic measurements. The main difference is in the measurement procedure: once the sample is prepared it should be kept under stirring for 20 min, and then the extinction spectrum is measured. For each spectrum the integral in the range of 340 nm to 800 nm was calculated, and then plotted as a function of the Biot-IgG or antigen concentration, respectively. In every case the linear fitting gave a R^2 value

above 0.99, and the calibration curve fitting gave a R^2 value above 0.98.

Clinical samples

Serum samples used in this study were obtained from healthy control individuals (n = 17) and patients with RA (n = 45) recruited from the Rheumatology Unit, Hospital Nacional de Clínicas, Universidad Nacional de Córdoba, Argentina. The local Ethics Committee Board approved the study and patients signed an informed consent before participation. Diagnosis of RA was established by a rheumatologist on the basis of the criteria established (2010) by the American College of Rheumatology/European League Against Rheumatism.[27] The control group showed no signs of RA and did not report any autoimmune or immune-mediated disorders, which was confirmed by clinical and laboratory evaluations. Blood samples were collected by venipuncture into tubes without anticoagulant. Each blood sample was allowed to clot for 30 minutes before the serum was processed. After centrifugation for 15 minutes at 2500 rpm, the serum was collected by pipetting and placed in labeled Eppendorf microtubes and stored at −80 °C until use.

Microplate reader measurements

For selecting the regime where dimer formation is favored, 0.1 mL of the functionalized Ag NPs were added to PBS (final volume of 0.3 mL). For these experiments, different amounts of biotinylated anti-human TNFα IgG were added directly to the mixture of Ag NPs and the buffer (regarding the final volume of 0.3 mL). For calibration experiments, a specific amount of Biot-IgG (0.3 ng mL^{-1}) and different amounts of antigen (TNFα) were added directly to the mixture of Ag NPs, biotinylated anti-human TNFα IgG and the buffer. The biotinylated anti-human TNFα IgG concentration was chosen in order to be in the regime where dimer formation is favored. The intensity was monitored with a microplate reader spectrophotometer using a 415 nm filter. The intensity (buffer corrected) was plotted as a function of the Biot-IgG or antigen concentration, respectively. The calibration curve in the whole concentration range was adjusted to an exponential function ($I = -A_0e^{-b\times C} + I_0$) where I = intensity and C = concentration, and the fitting gave a R^2 value above 0.9, alternatively the linear range of the calibration curve can be used for quantifying and the optimization gave a R^2 value above 0.89. For clinical sample measurements, dilutions of the real samples were performed: 2 μL of a 1 : 10 dilution of the serum was added to the mixture of Ag NPs, Biot-IgG and buffer (final volume 0.3 mL). The intensity, after corrected according to the buffer and the serum intensity, was used to calculate the antigen (TNFα) concentration in the real samples using the equation obtained from the fitting of the experimental data.

Quantification of TNFα in human serum by ELISA

TNFα concentration in human serum samples was also quantitated by a commercially available solid phase sandwich ELISA kit according to the manufacturer's instructions (Human TNF-α ELISA MAX™ Standard; BioLegend, San Diego, CA, USA). In detail, 96-well microplates were coated with a primary anti-human TNFα capture antibody (100 μl per well), sealed, and incubated overnight between 2 °C and 8 °C. Wells were washed 4 times with washing buffer (0.05% Tween-20-supplemented PBS) and then blocked with 5% BSA-supplemented PBS (200 μl per well) for 1 h at room temperature with shaking. Wells were washed 4 times with washing buffer and standards and serum sample dilutions were added to the appropriate wells (100 μl per well). Plates were sealed and incubated at room temperature for 2 h with shaking. Then after washing the wells 4 times, the biotinylated anti-human TNFα detection antibody was added to every well (100 μl per well) and incubated at room temperature for 1 h with shaking. Wells were again washed 4 times and 100 μl of diluted avidin–horseradish peroxidase solution was added to each well, sealed and incubated at room temperature for 30 minutes with shaking. Wells were washed 6 times and 100 μl of TMB substrate solution were added to each well and incubated in the dark for 15–30 minutes or until the desired color developed. The reaction was stopped by adding 100 μl per well of Stop Solution (2 M H_2SO_4). Absorbance was read at 450 nm in a microplate reader (Bio-Rad) within 30 minutes. The amounts of TNFα were extrapolated from the standard curve, which was generated in 1/2 dilutions. Results are expressed in nanograms or picograms per milliliter.

Extinction measurements

The characterization by UV-Vis spectroscopy was carried out, scanning in the 200–1100 nm range. The spectra were recorded using a Shimadzu UV-1700 PharmaSpec spectrophotometer with a 1 cm quartz cell at room temperature.

Transmission electron microscopy

Transmission electron microscopy (TEM) images were obtained using a JEM-JEOL 1120 EXII under an accelerating voltage of 80 kV. Samples were prepared by adding one drop (~50 μL) of the sample colloidal solutions onto a holey carbon-formvar coated copper TEM grid (100 mesh).

Computational methods

The optical response of Ag NSs was computed using the Generalized Multiparticle Mie (GMM) theory as described elsewhere.[28–30] In all the calculations performed in this work the NPs were excited by a plane wave with an incidence pointing vector (propagation direction) normal to the surface. The angular average extinction cross-section denoted by σ_{EXT} has been computed averaged the extinction efficiency (Q_{EXT}) over 8 different polarizations (from 0° to 90°), and considering the effective area at each angle. In all the simulations, we have used the dielectric function tabulated by Palik for Ag and Au.[31]

Results and discussion

Design and principles of IDILA

The IDILA assay is based on the optical response of a colloidal dispersion of Ag nanospheres (NSs) and the strong interactions

of the streptavidin (STV)–biotin system combined with the highly specific biomolecular recognition ability of immunoglobulins (IgG), and can be completely applied only using a common UV-Vis spectrophotometer. Ag NSs are easily functionalized with the STV–biotin system mixing the reactants (NSs/STV/biotin) at a 1 : 1 : 1 ratio (Fig. 1A). The strict stoichiometric control is necessary due to the ability of the STV protein to interact with a maximum of four biotin molecules, which could induce the formation of NS aggregates.[14] According to this, the functionalization of 60 nm Ag NSs was performed by the addition of biotin simultaneously with the STV protein in an equal final concentration (ratio STV/biotin 1 : 1). The high kinetic and thermodynamic constants of biotin–STV interactions guarantee the formation of biotin–STV complexes avoiding a primary chemisorption of biotin molecules onto the NS surface which could lead to the formation of NS

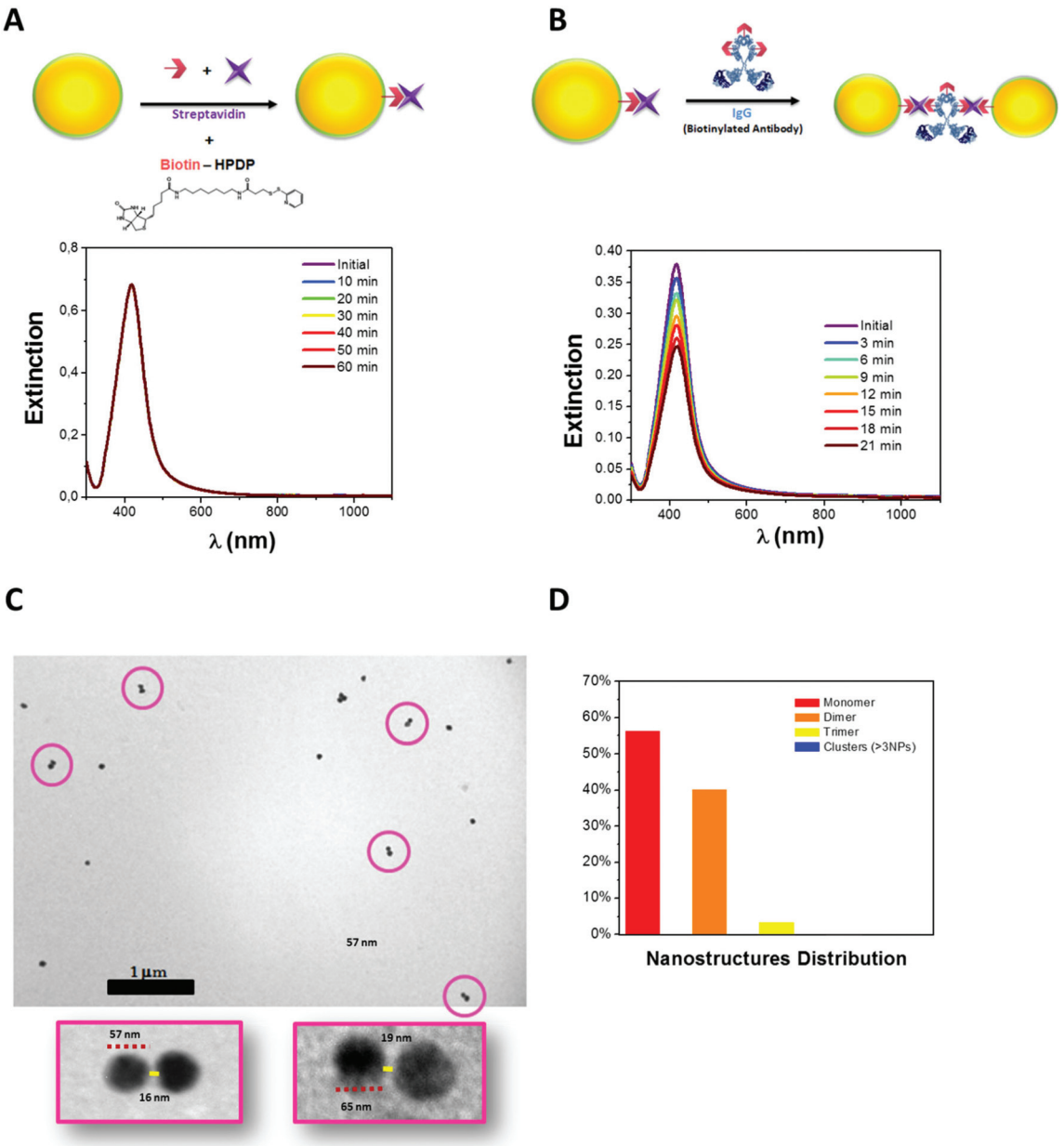

Fig. 1 Nanoparticle probes for IDILA. (A) Schematic representation of the nanoparticle functionalization strategy with the streptavidin (STV)–biotin system (top), and extinction spectra evolution of Ag nanoparticles functionalized with the STV–biotin system using a NP/STV/biotin 1 : 1 : 1 ratio. (B) Schematic representation of the nanoparticle controlled agglomeration strategy (dimer formation) in the presence of a biotinylated antibody (Biot-IgG), and extinction spectra evolution of functionalized Ag nanoparticles in the presence of 0.3 ng mL^{-1} of Biot-IgG. (C) Representative image of nanoparticle dimers, as observed by transmission electron microscopy (scale bar, 1000 nm). The pink circles highlight the dimers formed. (d) Histogram of the nanostructure distribution after 21 minutes of the addition of 0.3 ng mL^{-1} of Biot-IgG (it is shown as the percentage distribution over the 300 nanostructures).

aggregates (the interaction of the biotinylated NSs leads to the formation of random aggregates through H-bonds between biotins).[14,32]

The biosensor consists of a controlled agglomeration (formation of Ag NS dimers) in the presence of a biotinylated immunoglobulin G (Biot-IgG) acting as a linker between the NSs functionalized with the biotin–STV system (Fig. 1B). After 21 minutes of the addition of 0.3 ng mL^{-1} Biot-IgG the TEM statistics depicts only the formation of dimeric structures besides the presence of monomers, with almost negligible quantities of trimers (Fig. 1C and D). TEM analysis also reveals that the gap between NSs is around 20 nm (see Fig. 1C), which is in excellent agreement considering the linker molecules in the gap (distance biotin–STV–Biot-IgG–STV–biotin $\approx$ 20 nm) (see Fig. 2A). The biotin fragment length was calculated using quantum mechanical structure optimization (B3LYP method with 6-311++G(d,p) basis sets)[33] and the protein lengths were obtained from a protein data bank. The formation of the dimeric nanostructures is experimentally evidenced by a decrease in the intensity of the extinction spectra (*i.e.*, surface plasmon intensity depletion). As is known, the dipolar coupling in dimers will result in an intensity increase and especially in a redshift of the LSPR peak when the polarization of the incident radiation is able to generate the maximum coupling effect (oscillating E-field in the interparticle axis).[28,34,35] Nevertheless, the dimers in these experiments are in a colloidal dispersion with a random incident polarization. According to this, it is not accurate to consider the optical response when the maximum coupling effect is reached (*i.e.*, the electric field polarized along the interparticle axis). Instead, one must consider the optical response of a dimer averaged according to different incident polarizations.[36] In that sense, the theoretical spectrum of a 60 nm diameter Ag NS dimer with an interparticle distance of 20 nm was calculated by averaging the simulated extinction efficiency (Q_{EXT}) spectrum as a function of the angle between the dimer axis and the electric field of the incident radiation (θ). In addition, the effective geometrical area projected at each angle was considered in order to obtain the extinction cross-section (σ_{EXT}). This experimentally observed intensity depletion can be rationalized considering that the extinction spectra of 60 nm diameter Ag NS dimers with a 20 nm gap and the monomers follow a similar shape (considering the average polarization of dimers in solution), but the extinction cross-section of the dimers is lower than the monomers at the wavelength of the maximum of the monomer extinction spectrum (see left panel of Fig. 2B). This experimentally observed decrease in the maximum of the extinction spectrum is a consequence of dipolar plasmon resonance coupling between the nanoparticles. This coupling generates two different surface plasmon modes, which correspond to the longitudinal and transversal dipole modes.[28] For relative large interparticle distance (20 nm), these modes are very close in energy, generating an important decrease and only a small shift of the Q_{EXT} at the maximum coupling ($\theta = 0°$) with respect to the monomer Q_{EXT} (see right panel of Fig. 2B). A rather non-intuitive result is that when the angular average is considered, the shift effect is almost negligible but the drop in the intensity is notorious. Therefore, as the monomers are consumed the intensity drops as a consequence of the significant lower σ_{EXT} of the dimers. Fig. S1 in the ESI† shows that this depletion effect could be observed for 60 nm diameter Ag NS dimers with an interparticle distance of 20 nm but not when the interparticle distance decreases (*i.e.*, 2 nm gap generates a complex optical response in comparison with the extinction response of the monomer). Moreover, this effect is not expected to be observed even with 90 nm diameter Au NSs, as the coupling is weaker in Au in comparison to Ag (see Fig. S3 in the ESI†). In this respect, this phenomenon is extremely dependent upon the gap distance and on the metal nature and the size of the NPs. Therefore, a morphological characterization of the Ag NPs should be done before their functionalization for an IDILA assay.

In order to validate the physical origin of this phenomenon, theoretical simulations of the experiment were performed combining the simulated extinction cross-section of the monomers and dimers (see left panel of Fig. 2B) and the statistical analysis obtained by a direct count of the number of dimers and monomers observed in several TEM images. The images correspond to the nanostructures present in the colloidal dispersion at 21 minutes after the addition of 0.3 ng mL^{-1} Biot-IgG (see Fig. 1D). The results indicate that at this time the composition of the sample consists of 40% of dimers and 60% of monomers. The decrease in the extinction intensity after 21 min is shown in the left panel of Fig. 2C. The initial concentration of the monomers was calculated using the experimental extinction intensity and the simulated extinction cross-section (initial = 1.25×10^9 NPs per mL (monomers)) considering a 1 cm optical path (Beer's law). The resulting simulated extinction spectrum of monomers and the initial experimental extinction spectrum are shown in the right panel of Fig. 2C. The concentration of monomers and dimers after 21 min after the addition of Biot-IgG was estimated considering the relative weights of monomers and dimers obtained from the statistical analysis described above (after 21 min = 0.75×10^9 NPs per mL (monomers) + 0.5×10^9 NPs per mL (dimers) = 0.75×10^9 monomers per mL + 0.25×10^9 dimers per mL). The simulated extinction spectra of monomers and dimers were calculated using the respective extinction cross-sections and concentrations (see right panel of Fig. 2C). The resulting simulated extinction spectrum (extinction spectrum of 40% dimers + extinction spectrum of 60% monomers) and the experimental extinction spectrum of nanostructures formed after 21 minutes of the addition of 0.3 ng mL^{-1} Biot-IgG are also shown in the right panel of Fig. 2C. As can be appreciated, there is an excellent correlation between the simulated total extinction spectrum and the experimental one. This agreement constitutes a very stringent test concerning the theoretical interpretation of the depletion phenomenon observed under the real experimental conditions employed.

The temporal variation of the extinction spectrum (intensity depletion) allows one to obtain the apparent agglomeration rate constant (k_{Aglo}) for the dimer formation as a function of

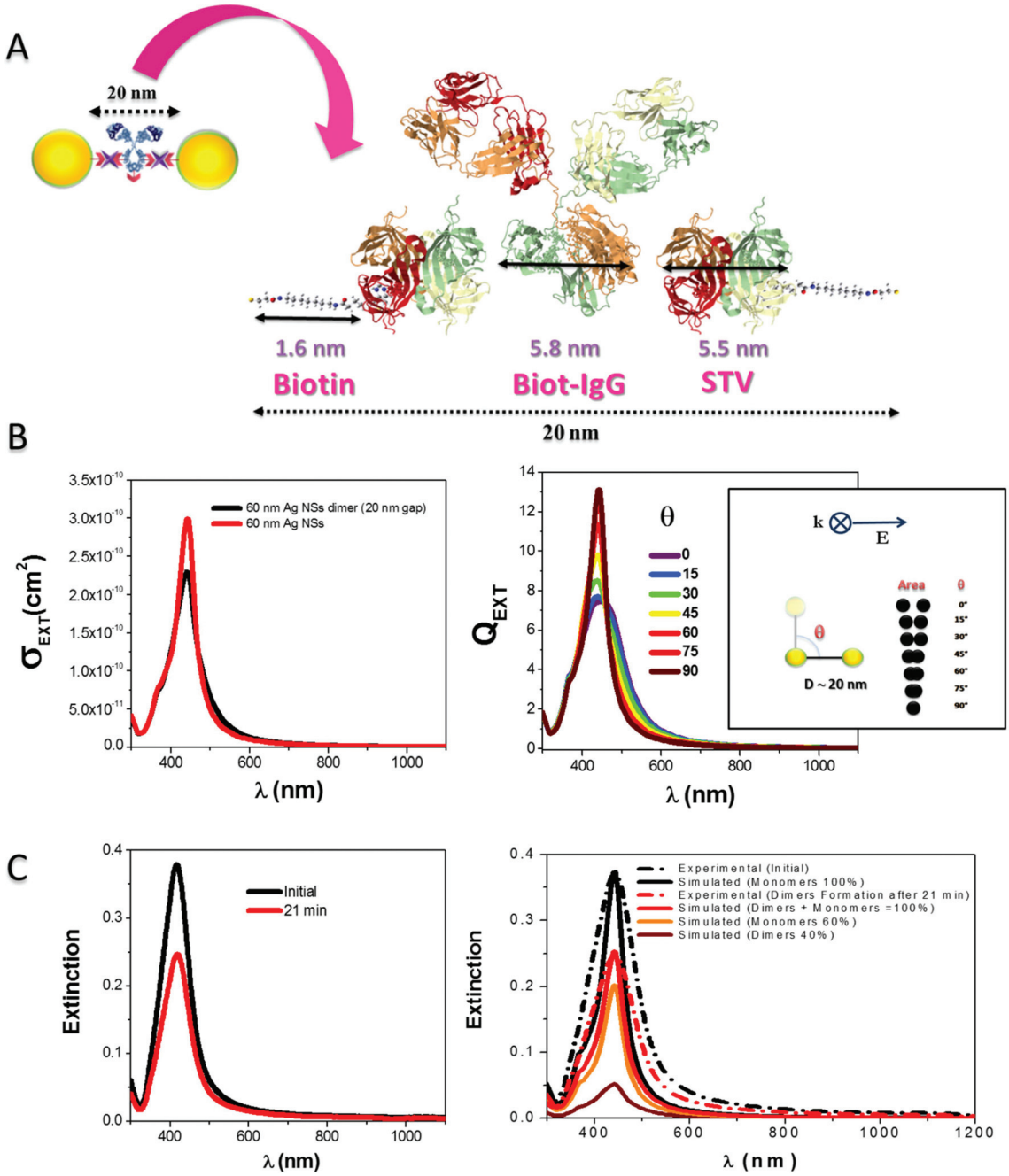

Fig. 2 Theoretical interpretation. (A) Structural parameters of the molecules in the gap of the dimers formed by the addition of Biot-IgG to a colloidal dispersion of functionalized Ag NPs. Biotin fragment length was calculated using quantum mechanical structure optimization and the protein lengths were obtained from a protein data bank. (B) Average simulated extinction cross-section (left panel) and extinction efficiency of the dimer at different orientations (averaged over 8 different orientations) (right panel). As the dimers are in a colloidal dispersion with a random incident polarization, the theoretical spectrum must be calculated by averaging the simulated extinction efficiency (Q_{EXT}) spectrum as a function of the angle between the dimer axis and the electromagnetic field of the incident radiation (θ), and considering the effective geometrical area projected at each angle (inset in right panel). (C) The left panel shows the experimental extinction spectra of the Ag nanoparticles before (solid black line) and after 21 min of the addition of 0.3 ng mL^{-1} of Biot-IgG (solid red line). The right panel compares the initial and final (21 min) experimental extinction spectra with electrodynamics simulations. The initial spectrum considering 100% of monomers is depicted with a black dashed line and the calculated one is shown with a black solid line. There is an excellent agreement between the calculated extinction spectra (solid red line) and the experimental extinction spectra (red dot dashed line) after 21 min considering for the calculation that the spectra at this time is the sum of the relative contribution of the spectra corresponding to a relative population of 40% of dimers (solid brown line) and 60% of monomers (solid orange line). The percentages were obtained by statistics of TEM images.

Biot-IgG concentration (Fig. 3A left panel). The temporal decrease in the intensity of the extinction is dependent upon the concentration of Biot-IgG used: as Biot-IgG increases, the absolute value of k_{Aglo} first increases, reaches a maximum, and then decreases again (Fig. 3A right panel). The attenuation of the dimer formation (low absolute value of k_{Aglo}) occurs when the Biot-IgG concentration is so high that under this condition most of the STV-binding-sites of the NSs are bound to individual Biot-IgG molecules and do not form dimers. The regime relevant to apply the IDILA method is the one where the concentration of Biot-IgG guarantees that the process of dimer formation is favored. In this case, in the presence of the antigen of interest, an inhibition of the formation of dimeric structures is observed, evidenced by the decrease in the absolute value of

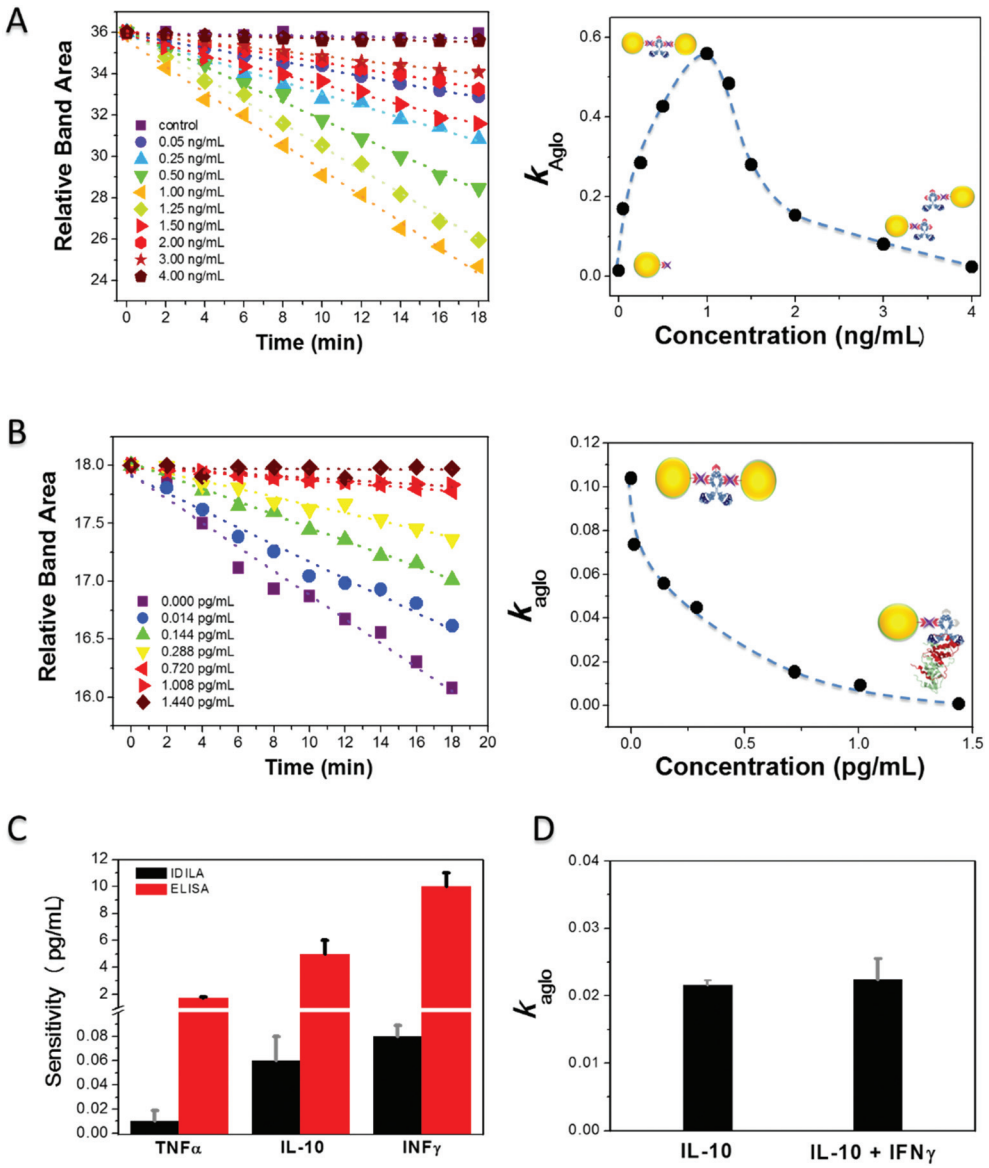

Fig. 3 IDILA principles for antigen quantification. (A) Relative band area of the extinction spectrum (integral from 340 to 800 nm) as a function of time of Ag nanoparticle dispersions in the presence of increasing amounts of a biotinylated antibody (Biot-IgG) (left panel), and dimer formation rate constant (k_{Aglo}) as a function of Biot-IgG concentration (using anti-IFNγ) (right panel). In every case the blue dotted line is a guide to the eye, and the concentrations given are final concentrations in the assay. (B) Relative band area of the extinction spectrum as a function of time for Ag nanoparticle dispersions in the presence of 0.3 ng mL^{-1} of anti-IFNγ and increasing amounts of antigen (IFNγ) concentration (left panel), and dimer formation rate constant (k_{Aglo}) as a function of IFNγ concentration. (C) Comparison of the sensitivity of IDILA and ELISA. Bar plot of the limit of detection of antigens using IDILA and the corresponding values of commercially available ELISA kits. The antigens used were tumor necrosis factor alpha (TNFα), interferon gamma (IFNγ) and interleukin 10 (IL-10). The Biot-IgG concentration was 0.3 ng mL^{-1} in all experiments. (D) Selectivity of IDILA. Bar plot of the dimer formation rate constant (k_{Aglo}) using IDILA of IL-10 alone or in a mixture with IFNγ. In both experiments the Biot-IgG used was anti-IL-10. Data are expressed as mean ± SD. The error bars were determined as the standard deviation of the values obtained with data fitting from two separate measurements. The Biot-IgG concentration was 0.3 ng mL^{-1} in all experiments.

k_{Aglo} (Fig. 3B left panel). This variation of the absolute value of k_{Aglo} with the antigen concentration allows one to obtain calibration curves and quantify the specific antigen (Fig. 3B right panel). The same kinetics behavior for dimer formation as a function of Biot-IgG concentration and the inhibition of the formation of dimeric structures in the presence of the antigen was evidenced for all the Biot-IgGs studied (anti-rabbit IgG, anti-mouse IL-10, anti-mouse IFNγ and anti-human TNFα) and the corresponding antigens (rabbit IgG, recombinant mouse IL-10, recombinant mouse IFNγ and recombinant human TNFα) (see Fig. 3 and 4 and ESI Fig. S3 and S4†). A similar behavior is observed despite the great differences in the antigen dimensions with lengths encompassing the range of 2.7–14.9 nm. This feature suggests that the inhibition process seems to be applicable to almost any Biot-IgG-specific antigen pair (Fig. S5†).

The evaluation of the analytical parameters of the biosensor for the antigens of clinical relevance of this study is presented in Table 1. A comparison of the detection sensitivity of IDILA

Table 1 Analytical parameters of IDILA

	TNFα	IL-10	IFNγ
Sensitivity	(0.011 ± 0.009) pg mL^{-1}	(0.06 ± 0.02) pg mL^{-1}	(0.078 ± 0.009) pg mL^{-1}
LOD	0.3 pg mL^{-1}	0.8 pg mL^{-1}	0.4 pg mL^{-1}
LOQ	1.0 pg mL^{-1}	3.3 pg mL^{-1}	1.1 pg mL^{-1}

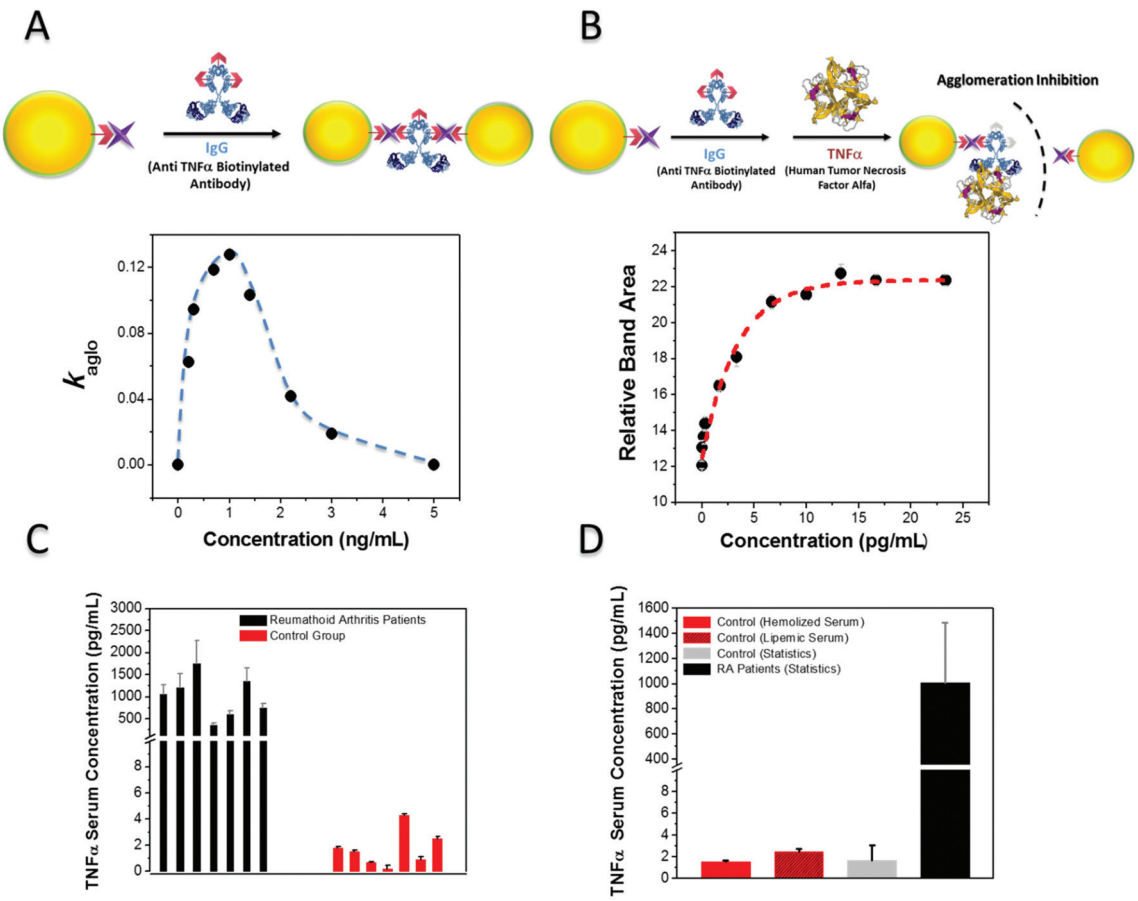

Fig. 4 Static IDILA measurements for antigens quantification. (A) Schematic representation of the nanoparticle controlled agglomeration strategy (dimer formation) in the presence of a biotinylated antibody (Biot-IgG), and plot of the dimer formation rate constant (k_{Aglo}) as a function of Biot-IgG concentration (using anti-human TNFα). The blue dotted line is a guide to the eye. Concentrations given are final concentrations in the assay. (B) Schematic representation of the dimer formation avoided in the presence of the specific antigen (TNFα), and calibration curve of the antigen (TNFα) in the presence of the specific Biot-IgG (final concentration of 0.3 ng mL^{-1}). Concentrations given are final concentrations in the assay. The corresponding area of the extinction spectrum (from 340 to 800 nm) for each final concentration of antigen was measured after 20 min of the addition of the reagents. The red dotted line is the curve fitting of the experimental data (R^2 > 0.98). The equation of this fitting was used to quantify the real samples. (C) Diagnosis of clinical samples. Clinical serum specimens (50 μL for each sample) of rheumatoid arthritis patients and healthy subjects were directly added to the mixture of reagents and the area of the extinction spectrum for each final concentration of antigen was measured after 20 min of the addition of the reagents. The error bars were determined as the standard deviation of the values obtained with data fitting from two separate measurements. (D) Reliability of the analysis. Inadequate/suboptimal (lipemic or hemolyzed) serum specimens of healthy subjects were measured under the same conditions as the other serum specimens and the results are compared with the average value of antigen (TNFα) of RA patients and the average value of healthy subjects (control group statistics). Data are expressed as mean ± SD.

Table 2 Comparison of IDILA and ELISA for antigen detection

			IDILA		ELISA
Sensitivity	TNFα		(0.011 ± 0.009) pg mL^{-1}		(1.7 ± 0.1) pg mL^{-1} [a]
	IL-10		(0.06 ± 0.02) pg mL^{-1}		(5 ± 1) pg mL^{-1} [a]
	IFNγ		(0.078 ± 0.009) pg mL^{-1}		(10 ± 1) pg mL^{-1} [a]
		Sample number	IDILA quantification	Sample number	ELISA quantification
Serum samples	RA patients	1	(1.7 ± 0.3) ng mL^{-1}	8	(1.96 ± 0.08) ng mL^{-1}
		2	(0.36 ± 0.05) ng mL^{-1}	9	(0.41 ± 0.02) ng mL^{-1}
		3	(0.60 ± 0.09) ng mL^{-1}	10	(0.40 ± 0.02) ng mL^{-1}
		4	(1.4 ± 0.3) ng mL^{-1}	11	(1.38 ± 0.03) ng mL^{-1}
		5	(0.7 ± 0.1) ng mL^{-1}	12	(0.25 ± 0.02) ng mL^{-1}
		6	(1.1 ± 0.2) ng mL^{-1}	13	(1.13 ± 0.03) ng mL^{-1}
		7	(1.2 ± 0.3) ng mL^{-1}	14	(1.95 ± 0.07) ng mL^{-1}
	Control group	1	(1.8 ± 0.1) pg mL^{-1}	8	(3 ± 1) × 10^{1} pg mL^{-1}
		2	(1.5 ± 0.1) pg mL^{-1}	9	N.D.
		3	(2.5 ± 0.2) pg mL^{-1}	10	(5 ± 1) × 10^{1} pg mL^{-1}
		4	(0.7 ± 0.1) pg mL^{-1}	11	N.D.
		5	(4.3 ± 0.1) pg mL^{-1}	12	(9 ± 2) × 10^{1} pg mL^{-1}
		6	(0.2 ± 0.1) pg mL^{-1}	13	N.D.
		7	(0.9 ± 0.2) pg mL^{-1}	14	N.D.

[a] Data of commercially available ELISA kits from Thermo Fisher Scientific.

and the sensitivity informed in commercially available ELISA kits is shown in Fig. 3C. Titration experiments revealed that the average sensitivity was ≈0.05 pg mL^{-1} (see Tables 1 and 2 for details), which implies 80–160 fold enhancement in the sensitivity over the traditional colorimetric ELISA. Moreover, the specificity of the detection was tested in the simultaneous presence of the different interleukins (Fig. 3D), showing a remarkable performance for specific sensing. In addition, the system presents an outstanding stability with phosphate buffer solution (PBS) supplemented with 5% of bovine serum albumin (BSA), and also in the presence of real clinical samples as normal, lipemic and hemolyzed blood serum specimens (ESI Fig. S6†). The stability analysis of the colloidal dispersion in phosphate buffer media (pH = 7.2–7.4) and clinical samples (pH = 7.0–7.5) shows that the optical response is a consequence of the functionalization strategy in combination with the immunorecognition properties of biotinylated antibodies and not because of an uncontrolled agglomeration process due to the biological matrices.

Clinical testing

Moving forward, we adapted the assay described above as a generic platform to effectively detect and quantify antigens in samples in a much more simple way without the need of a kinetic analysis by performing a straightforward measurement. As the intensity depletion is the relevant process, we discovered that a calibration curve can be obtained just by measuring the integral of the extinction spectra between 340 and 800 nm 20 min after the addition of Biot-IgG and different amounts of the antigen, under continuous stirring (Fig. 4A and B, respectively).

A challenge test of this methodology was performed by evaluating the clinical utility of IDILA using RA patient specimens. Aspirated serum samples from patients with RA were collected and analyzed by conventional ELISA as well as by IDILA in order to quantify the presence of TNFα, a cytokine mainly produced by macrophages, which have been implicated in the pathogenesis of RA.[37] Fig. 4C shows the results from IDILA. To place these findings in perspective, Table 2 shows a comparison of the IDILA results with those obtained using the standard ELISA methodology. As it is evident from the data shown in this table, IDILA showed excellent accuracy, detecting minimal changes both in the RA patients as well as in the control group. We also demonstrate that IDILA can be performed in inadequate/suboptimal specimens such as lipemic or hemolyzed serum samples, without giving false positive results (Fig. 4D).

Taking IDILA to clinical laboratories

Common colorimetric ELISA is measured using a microplate photometer usually with a 96-well microplate (8 by 12 matrix) with a typical reaction volume between 100 and 200 μL per well. Here we take one step forward and demonstrate that IDILA can be adapted to perform the measurements with the same equipment that biochemistry laboratories currently use for ELISA determinations. The advantage of this novel methodology is that as the measurements are performed in colloidal dispersion, it does not require high amounts of reagents to be immobilized, implying short experiment lengths and extremely low amounts of reagents (*i.e.*, lower price per experiment – see ESI Table S1†). The experiment performed with the microplate consists of the simultaneous mixing of 100 μL of Ag NPs functionalized with the STV–biotin system (Fig. 5A) with different volumes of the standard antigen or the real sample, and PBS to achieve a final volume of 300 μL per well. After a 20 min incubation the intensity

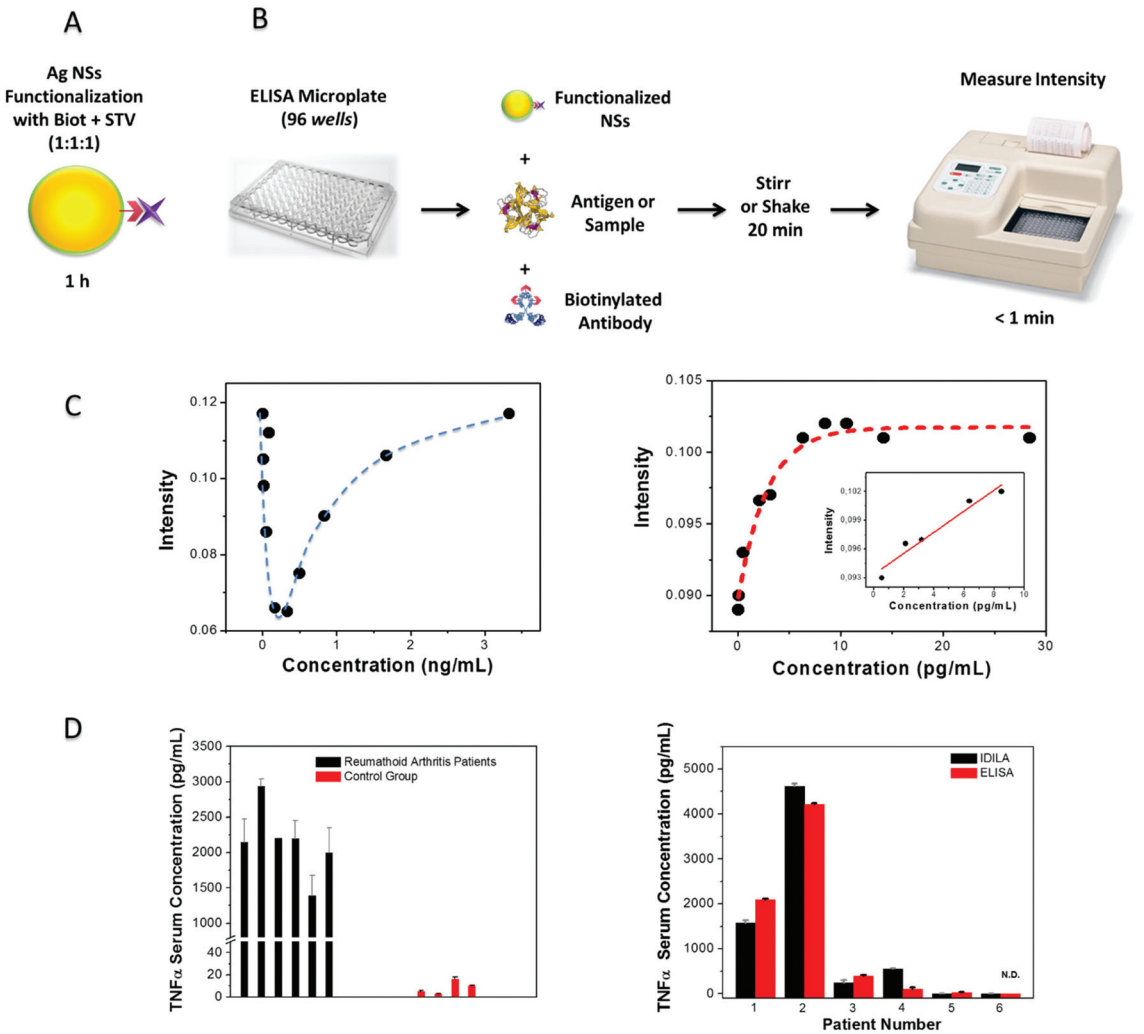

Fig. 5 Measuring antigens in clinical samples with IDILA using common biochemical equipments. (A) Schematic representation of the nanoparticle functionalization strategy. (B) Schematic representation of the IDILA assay procedure. The functionalized NPs are added to the ELISA microplate of 96 wells together with the specific biotinylated antibody (Biot-IgG), the recombinant antigen or the real sample. For the determination of the appropriate amount of Biot-IgG, a calibration could be performed just changing the final concentration of Biot-IgG at the same NP volume. For the calibration curve of the antigen the concentration of Biot-IgG and the volume of functionalized NPs remain the same while the concentration of the antigen is increased. For experiments with real samples, the same amount of NPs and Biot-IgG used in the calibration curve of the antigen is added to the microplate and then a specific amount of the real clinical sample is added. In every case the final volume is adjusted with buffer solution (final volume = 300 μL). (C) Calibration of the appropriate amount of Biot-IgG (left, using biotinylated anti-human TNFα) and calibration curve of the antigen (right, using recombinant human TNFα). The blue dotted lines are a guide for the eye. The red dotted line is the curve fitting of the experimental data ($R^2 > 0.95$). The equation of this fitting was used to quantify the real samples. The inset highlights the linear range that can be used for quantification. (D) Quantification of antigen in real clinical samples (right, using serum from rheumatoid arthritis patients and serum of healthy control subjects) and comparison between IDILA and ELISA for the same clinical samples. Concentrations given are final concentrations in the assay.

should be monitored with a microplate reader spectrophotometer using a 415 nm filter (registers the intensity at the LSPR wavelength of the NP monomer). The 96-well microplate allows performing the calibration curve and sampling measurements in the same experiment, which reduces its duration to less than 2 h, including the sample preparation and the stirring time (Fig. 5). Interestingly, the small reaction volume and the sensitivity of IDILA allow using clinical sample volumes in the order of 1 μL. Thus, the clinical implications of being able to detect antigens in a fast way with commonly used equipment and using small sample amounts are very significant as a diagnosis tool. Furthermore, by having the ability to detect antigens directly in the specimen, IDILA not only overcomes the problems of immobilization of reagents or uncontrolled enzymatic reactions, but also minimizes the possibility of sample contamination through the several steps of the ELISA methodology. Diagnostic accuracy is thus maximized. Whilst these results are encouraging, further in-depth studies with larger prospective clinical trials and standardization of analysis conditions would be needed to correctly extrapolate the methodology to common biochemistry laboratories.

Conclusions

In the current study, we designed an optical bionanosensing methodology capable of detecting antigens with unprecedented levels of sensitivity. The method is robust, fast (<2 hours), cheap, sensitive, accurate and potentially adaptable to any antigen. Therefore, it has the potential for guiding decisions in a more accurate way across various clinical scenarios, in particular clinical prognosis and diagnosis. Most of the routine methodologies used to detect and quantify antigens involve heterogeneous sensing (*i.e.*, immobilization of reagents) that demand several steps and consume high amounts of reagents, with the shortcoming that they could lead to sample contamination and are very time consuming. IDILA not only overcomes these issues, but also has several advantages:

• It does not involve any enzymatic reactions for target amplification or detection and does not need specific devices or equipment for reactions or storage of reagents.

• It offers a technological platform that can be easily applied to the clinic as well as other point-of-care settings. The assay format is similar to ELISA, which is widely used in laboratories and clinics, and it does not need specific instruments or training.

• It can be applied using common and widely-used equipment like UV-Vis spectrophotometers or microplate photometers, available in any biochemistry laboratory.

• Its high sensitivity (the minimum value that can be quantified goes down to 0.01 pg mL^{-1}) could be potentially used for early diagnosis or detection of antigens in diluted samples.

In view of the above, we envision that this generic approach could have far-reaching applications.

Author contributions

J. C. F. designed and performed the research, and wrote the manuscript. R. D. M. and E. A. C. designed the research and co-wrote the manuscript. E. A. C. provided overall guidance. R. D. M. provided guidance and assistance regarding the clinical studies and performed the ELISA measurements. All authors discussed the results and commented on the manuscript.

Acknowledgements

The authors acknowledge financial support from CONICET (PIP 112-201101-00430), FONCYT (PICT 2012-2286, PICT 2012-3094), SECYT-UNC and PME 1544 – 2006. J. C. F. acknowledges CONICET for being a recipient of a PhD fellowship.

References

1 A. Lernmark, *J. Clin. Invest.*, 2001, **108**, 1091–1096.
2 C. Castro and M. J. Gourley, *Allergy Clin. Immunol.*, 2009, **125**, 238–247.
3 K. Egerer, E. Feist and G.-R. Burmester, *Dtsch. Arztebl. Int.*, 2009, **106**, 159–163.
4 F. Renger, H. Bang, E. Feist, G. Fredenhagen, A. Natusch, M. Backhaus, G.-R. Burmester and K. Egerer, *Arthritis Res. Ther.*, 2010, **12**, 1–5.
5 S. X. Leng, J. E. McElhaney, J. D. Walston, D. Xie, N. S. Fedarko and G. A. Kuchel, *J. Gerontol., Ser. A*, 2008, **63**, 879–884.
6 S. D. Gan and K. R. Patel, *J. Invest. Dermatol.*, 2013, **133**, 1–3.
7 G. Baker, A. Lajtha, S. Dunn and A. Holt, *Handbook of Neurochemistry and Molecular Neurobiology: Practical Neurochemistry Methods*, Springer Science, New York, 2007, ch. 8.
8 E. Roduner, *Chem. Soc. Rev.*, 2006, **35**, 583–592.
9 K. L. Kelly, E. A. Coronado, L. L. Zhao and G. C. Schatz, *J. Phys. Chem. B*, 2003, **107**, 668–677.
10 K. H. Su, Q.-H. Wei, X. Zhang, J. J. Mock, D. R. Smith and S. Schultz, *Nano Lett.*, 2003, **3**, 1087–1090.
11 L. Gunnarsson, E. J. Bjerneld, H. Xu, S. Petronis, B. Kasemo and M. Käll, *Appl. Phys. Lett.*, 2001, **78**, 802–804.
12 P. K. Jain and M. A. El-Sayed, *J. Phys. Chem. C*, 2008, **112**, 4954–4960.
13 W. Rechberger, A. Hohenau, A. Leitner, J. R. Krenn, B. Lamprecht and F. R. Aussenegg, *Opt. Commun.*, 2003, **220**, 137–141.
14 J. C. Fraire, L. A. Pérez and E. A. Coronado, *ACS Nano*, 2012, **6**, 3441–3452.
15 J. C. Fraire, M. L. Masseroni, I. Jausoro, E. M. Perassi, A. M. Diaz Añel and E. A. Coronado, *ACS Nano*, 2014, **8**, 8942–8958.
16 J. Wang, S. V. Boriskina, H. Wang and B. M. Reinhard, *ACS Nano*, 2011, **5**, 6619–6628.
17 J. Wang, X. Yu, S. V. Boriskina and B. M. Reinhard, *Nano Lett.*, 2012, **6**, 3231–3237.
18 G. X. Rong, H. Y. Wang, L. R. Skewis and B. M. Reinhard, *Nano Lett.*, 2008, **8**, 3386–3393.
19 M. J. Crow, G. Grant, J. M. Provenzale and A. Wax, *Am. J. Roentgenol.*, 2009, **192**, 1021–1028.
20 J. Aaron, K. Travis, N. Harrison and K. Sokolov, *Nano Lett.*, 2009, **9**, 3612–3618.
21 R. De la Rica and M. M. Stevens, *Nat. Nanotechnol.*, 2012, **7**, 821–824.
22 L. Rodriguez-Lorenzo, R. De la Rica, R. A. Álvarez-Puebla, L. M. Liz-Marzán and M. M. Stevens, *Nat. Mater.*, 2012, **11**, 604–607.
23 S. Mayilo, M. A. Kloster, M. Wunderlich, A. Lutich, T. A. Klar, A. Nichtl, K. Kürzinger, F. D. Stefani and J. Feldmann, *Nano Lett.*, 2009, **9**, 4558–4563.
24 S. Tang and I. Hewlett, *J. Infect. Dis.*, 2010, **201**, S59–S64.
25 C. Wang, M. Luconi, A. Masi and L. Fernandez, Silver Nanoparticles as Optical Sensors, in *Silver Nanoparticles*, ed. D. P. Perez, 2010, ISBN: 978-953-307-028-5.
26 C. A. Dinarello, *Eur. J. Immunol.*, 2007, **37**, S34–S45.
27 D. Aletaha, T. Neogi, A. J. Silman, J. Funovits, D. T. Felson, C. O. Bingham, N. S. Birnbaum, G. R. Burmester,

V. P. Bykerk, M. D. Cohen, *et al.*, *Ann. Rheum. Dis.*, 2010, **69**, 1580–1588.
28 E. R. Encina and E. A. Coronado, *J. Phys. Chem. C*, 2010, **114**, 3918–3923.
29 E. R. Encina and E. A. Coronado, *J. Phys. Chem. C*, 2010, **114**, 16278–16284.
30 E. R. Encina and E. A. Coronado, *J. Phys. Chem. C*, 2011, **115**, 15908–15914.
31 *Handbook of Optical Constant of Solids*, ed. E. D. Palik, Academic Press, New York, 1985.
32 J. C. Fraire, L. A. Pérez and E. A. Coronado, *J. Phys. Chem. C*, 2013, **117**, 23090–23107.
33 M. J. Frisch, G. W. Trucks, H. B. Schlegel, G. E. Scuseria, M. A. Robb, *et al.*, *Gaussian 98, Revision A.7*, Gaussian, Inc., Pittsburgh, PA, 1998.
34 L. Gunnarsson, T. Rindzevicius, J. Prikulis, B. Kasemo, M. Käl, S. Zou and G. C. Schatz, *J. Phys. Chem. B*, 2005, **109**, 1079–1087.
35 F. Chen, N. Alemul and R. L. Johnston, *AIP Adv.*, 2001, **1**, 03213.
36 J. C. Fraire, V. N. Sueldo Ocello, L. G. Allende, A. V. Veglia and E. A. Coronado, *J. Phys. Chem. C*, 2015, **119**, 8876–8888.
37 V. A. Danis, G. M. Franic, D. A. Rathjen, R. M. Laurent and P. M. Brooks, *Ann. Rheum. Dis.*, 1992, **51**, 946–950.